Supplementary Material

Polyurethane/Li$_{10}$GeP$_2$S$_{12}$ composite electrolyte with high ions transfer number and ions capture for all-solid-state lithium batteries

Peng Cui, Chun Sun, Wei Wei*

College of Electronic and Optical Engineering, Nanjing University of Posts&Telecommunications, Nanjing 210023, Jiangsu, China.

Correspondence to: Prof. Wei Wei, College of Electronic and Optical Engineering, Nanjing University of Posts&Telecommunications, 9 Wenyuan Road, Nanjing 210023, Jiangsu, China. E-mail: weiwei@njupt.edu.cn

SECTION 1
Materials

Polyether polyols (PPG, octahydroxy sucrose-oxide allyl ether, hydroxyl value: 450, Mw: 580-600), LiTFSI (bisfluoromethane sulfmide lithium, $C_2F_6LiNO_4S_2$, 99.99%), lithium hydroxide monohydrate (LiOH·H$_2$O，99.995%), acidic-nano-Al$_2$O$_3$ (99.9%, d = 5-10 nm), diphenylmethane diisocyanat (MDI, 98%, $C_{15}H_{10}N_2O_2$), and Li$_{10}$GeP$_2$S$_{12}$(LGPS, Mw:589, d = 1-5 μm), all raw materials, are provided by Aladdin, China, and directly applied without undergoing further purification process.

Fabrication of the composite electrolyte[(PU-LGPS)/Li$^+$, PLL]

PPG 20 g (0.03 mol) was added into a 50 mL beaker, followed by heating to 90 ℃ with stirring. 5 g (0.1 mol) LiOH·H$_2$O was dissolved with 5 mL deionized water for the preparation of the stationary aqueous solution at a concentration of 1 g/mL. Then the LiOH solution was added to beaker to react with PPG and heated to 120 ℃ and keep temperature to remove water at high temperature for 36 hours(noting: in this step that the water must be removed, otherwise the PU cannot be formed with the MDI). Then, LiTFSI 1 g (3 mmol) and 0.05 g (0.4 mmol) Al$_2$O$_3$ were added and stirred for 2 h until completely dissolved. Next, add 5 g(8 mmol) LGPS particles and stir the solution evenly to form a homogeneous solution. Then the 7.5 mmol MDI was added.　Finally, put 0.1ml PLL

emulsion into the mold of button cell shell of CR2016 to form PU at room temperature. The sample was then dried in a vacuum oven at 120 °C for 48 h (the operating loss error of this step is 0.2%).

Structure characterization

SPE morphology was observed using the field emission scanning electron microscope (ZEISS sigma500). The FTIR spectra were obtained by using the Fourier transform infrared spectrophotometer (PerkinElmer Spectrum Two). The Raman spectra were obtained by using the Japan -Horiba Scientific -LabRAM HR Evolution. The TGA/DSC data were documented by using Mettler DSC3, with temperature range: 10–1000 °C, heating rate of 10 K min^{-1}, under N_2. The stress–strain property was evaluated by using the ZQ-990 series universal testing machine. All samples for evaluation have a dimension of 20 mm (W) ×50 mm (L)×0.035 mm (H). The X-ray photoelectron spectroscopy (XPS) was obtained by using the United States-Thermofisher Nexsa machine.

Battery assembly and measurements

Ionic conductivity measurements based on alternating current impedance spectroscopy were performed in the CHI660e electrochemical workstation at a frequency of 100 kHz to 0.1 Hz and an oscillation potential of 10 mV. Composite electrolyte samples about 300 mm thick were sandwiched amid two metal sheet steels for the formation of test cells. The ionic conductivity can be expressed as follows:

$$\sigma=L/R_bS \tag{S1}$$

where σ refers to the ionic conductivity, R_b means the bulk resistance, L represents the thickness of electrolyte membranes, and S denotes the stainless-steel electrode area. All-solid-state lithium batteries adopted LiFePO$_4$ as the cathode and lithium metal as the anode for assembly, and the corresponding charge–discharge and cycling performance were investigated by using the LANHE CT2001A device.

Theoretical calculation

The influence of the functional groups on ion conductivity of the system was calculated

and analyzed by using the Vienna abinitio simulation package (VASP). The first-principles calculations under density functional theory (DFT) were carried out with the spin-polarized generalized gradient approximation (GGA). Core electron states were denoted by using the projectoraugmented-wave technique applied by VASP.[1-3] The exchange–correlation interactions were processed by using the GGA parameterized by Perdew, Burke, and Ernzerh (PBE) and represented by a plane wave with a wavefunction cutoff energy of 400 eV. The electronic wave function was converged to a tolerance of 10^{-5} eV (EDIFF = 10^{-5}), whereas the geometric optimization tolerance was taken as 0.05 eV/Å (EDIFFG = −0.05).

Supplementary Figure 1. Infrared and Raman characterization of PU and (PU+LGPS). (a) Infrared spectra of PU and with different LGPS contents; (b)Raman spectra of PU and (PU+LGPS).

The "black line" in **Supplementary Figure 1.** shows the Infrared spectra of sample PU .Firstly, by analyzing the Infrared spectrum of PU, it can be seen that the absorption peak at 3665 cm^{-1} can be attributed to the stretching vibration peak of "−NH" in PU[4]. The absorption peak at 3305 cm^{-1} is "−OH" stretching vibration peak in PU. The absorption peaks at 2978 cm^{-1} and 2867 cm^{-1} are asymmetric stretching vibration peaks of "−CH₃" and symmetrical stretching vibration peaks of "−CH₂" in the alkane structure of PU, respectively. The absorption peak at 2272 cm^{-1} is related to the asymmetric stretching vibration peak of isocyanate group ("−NCO") in PU [5].The

absorption peak at 1704 cm^{-1} is the stretching vibration peak of free carbonyl group ("—C=O") in PU. The absorption peak at 1599 cm^{-1} is "—C=C" stretching vibration peak in aromatic ring skeleton [4]. The absorption peak at 1538 cm^{-1} is the amide II band [6]. The absorption peak at 1509 cm^{-1} is related to the asymmetric stretching vibration of "—NH". The absorption peak at 1411 cm^{-1} is related to the shear vibration of "—CH$_2$" and asymmetric bending vibration of "—CH$_3$". The absorption peak at 1310 cm^{-1} is "—C—N" stretching vibration peak (amide III band)[6]. The absorption peak at 1226 cm^{-1} is the stretching vibration peak of "—C—O" in the ester group. The absorption peak at 1077 cm^{-1} is "—C—O—C" stretching vibration peak. The absorption peaks at 1014 cm^{-1} are "—C—O deformation vibration peak and "—C—H" swing vibration peak. The absorption peak at 812 cm^{-1} is related to the plane bending vibration peak of aromatic ring [6]. The absorption peak at 761 cm^{-1} was related to the in-plane oscillation peak of "—C—H$_2$", which indicated that PU material was successfully synthesized.

In order to further analyze the interaction between PU and LGPS, we changed the content of LGPS in PU-LGPS and analyzed the interaction between them by Infrared spectra. The "red line", "blue line" and "green line" in **Figure 1(a)** are three groups of samples with different proportions of LGPS addition. It can be seen that the absorption peak at 3382 cm^{-1} is related to the stretching vibration peak of "—OH" in PU. However, compared with PU, the stretching vibration peak of "—NH" and the asymmetric stretching vibration peak of isocyanate group ("—NCO") do not appear in the composite. The positions of other absorption peaks are similar to PU lines. In addition, the absorption peak intensity of the three materials also changed after the addition of LGPS. The intensity of absorption peaks near 1722 cm^{-1}, 1599 cm^{-1}, 1538 cm^{-1}, 1509 cm^{-1}, 1411 cm^{-1}, 1310 cm^{-1}, 1226 cm^{-1}, 812 cm^{-1} and 761 cm^{-1} decrease with the increase of LGPS, indicating that the strength of some functional groups in the composite decreases with the increase of LGPS.It is also further proved that the addition of LGPS weakens the coupling of polar functional groups to Li$^+$ and releases a large number of free Li$^+$, thus improving the conductivity of the composite electrolyte system (**Supplementary Figure 1 (b)**).
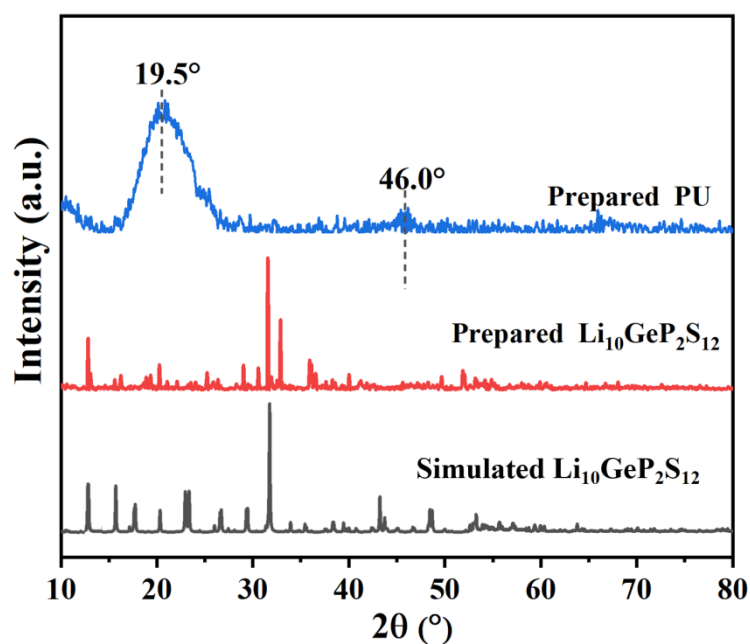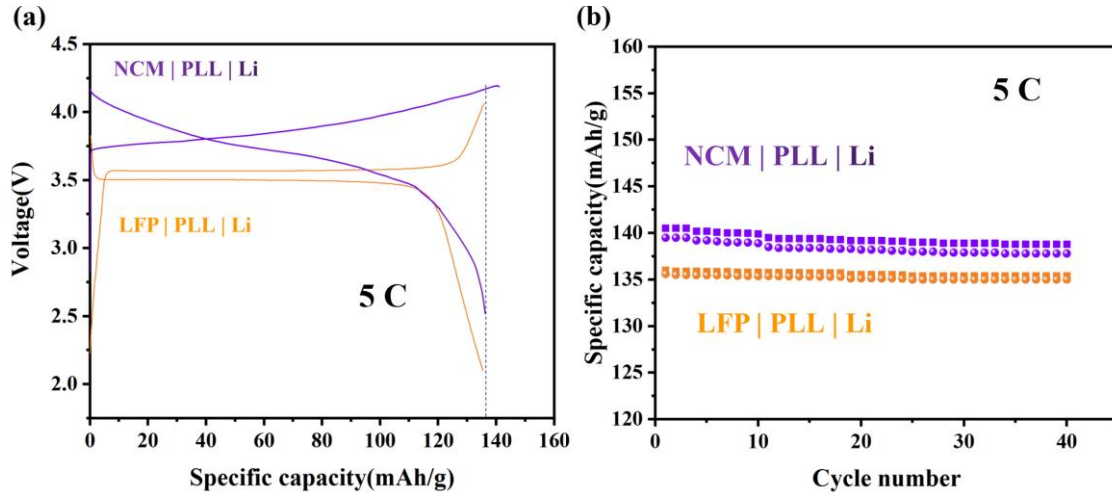
Supplementary Figure 2. XRD patterns of PU and LGPS.
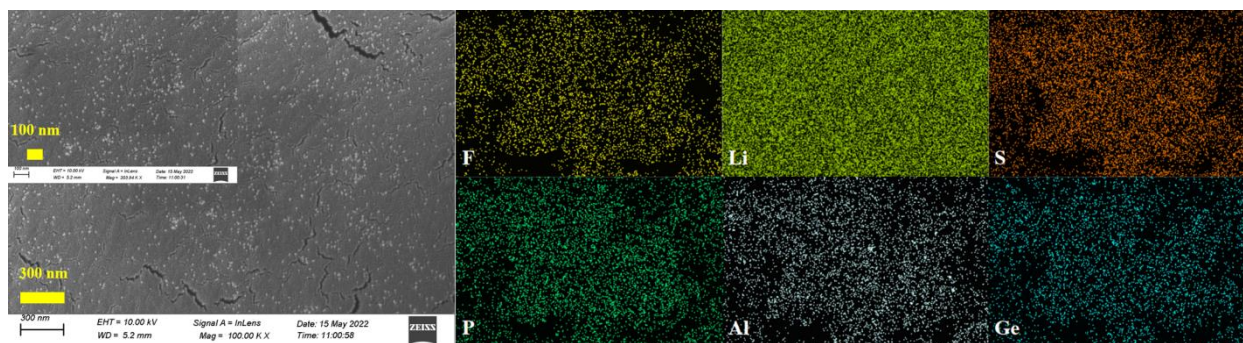
Supplementary Figure 3. The surface morphology SEM image and the elements mapping of PLL.
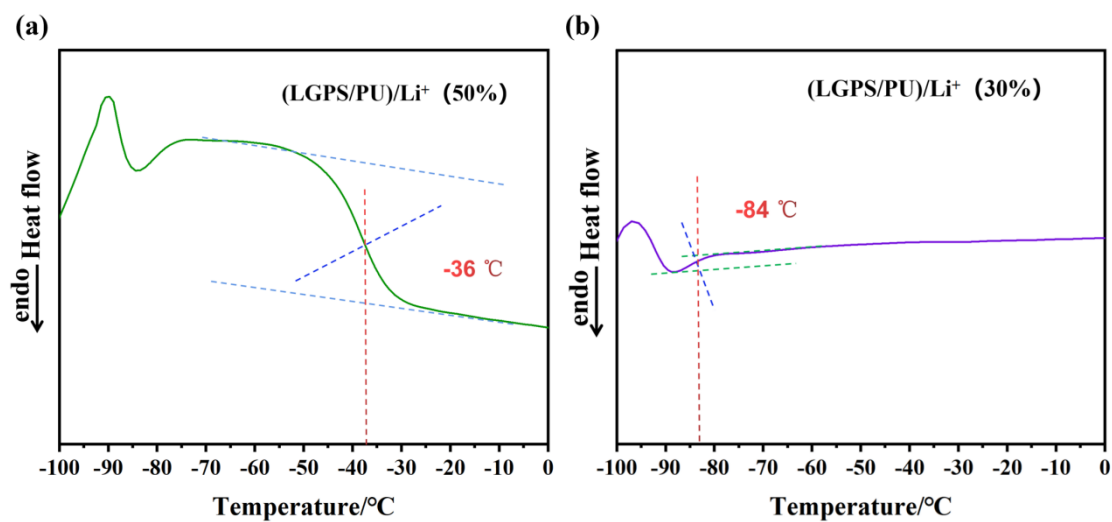
Supplementary Figure 4. (a) the Tg curves of (LGPS/PU)/Li$^+$(50%)**;(b)** the Tg curves of (LGPS/PU)/Li$^+$(30%);

Supplementary Figure 5. (a)The charge/discharge profiles of the NCM‖Li battery and LFP‖Li battery;(b) Comparison of the two batteries at 5 C.

The electrode NCM parameters are as follows: **(1)**Thickness of fluid collection(μm):16. **(2)** Concentration decent density(mg/cm^2) : 4.15. **(3)** Coating surface density(mg/cm^2): 21.6. **(4)** Active substance ratio: 96.5%. **(5)** Gram capacity of active material(mAh/g): 178. **(6)** Capacity of surface(mAh/cm^2):3.71. **(7)** Shelf life:One year (vacuum storage), after opening (used up in one month). **(8)** Gram capacity Description:25 ℃，0.1/0.1 C，3.0~4.3 V. **(9)** Electrode sheet size：10(cm)×10(cm).

SECTION 2: CALCULATION OF ACTIVATION ENERGY

The activation energy calculation is based on the Vogel-Tamman-Fulcher Equation, given below in terms of conductivity σ, the temperature T, an activation energy, *E*, and an empirical quantity with units of temperature, related to the glass transition T_g temperature and the activation volume. In a semiconducting polymer, this term should be strongly affected by local crystallinity, porosity, and any other effect which contributes to the volume change of the film upon ion intercalation

$$\sigma = T\sigma_0 \exp[-E/(T-T_g)] \tag{S2}$$

SECTION 3: CALCULATION OF IONIC TRANSFERENCE NUMBER

Then the ionic transference number of lithium ions, T_{Li^+}, for the composite can be calculated according to Equation (3):

$$T_{Li^+} = \frac{I_s(\Delta V - I_0 R_0)}{I_0(\Delta V - I_S R_S)} \tag{S3}$$

where ΔV is the polarization voltage, I_0 and R_0 are the initial current and resistance, I_s and R_s are the steady state current and resistance, respectively.

REFERENCES

1. Perdew JP, Burke K, Ernzerhof M. Generalized gradient approximation made simple. *Phys Rev Lett* 1996;77(18):3865. [DOI: 10.1103/PhysRevLett.77.3865]

2. Blöchl PE. Projector augmented-wave method. *Phys Rev B* 1994;50(24):17953. [DOI: 10.1103/PhysRevB.50.17953]

3. Hafner J. Ab-initio simulations of materials using VASP: Density-functional theory and beyond. *J Comput Chem* 2008;29(13):2044-78. [DOI: 10.1002/jcc.21057]

4. Badri KBH, Sien WC, Shahrom M, Hao LC, Baderuliksan NY, Norzali NR. FTIR spectroscopy analysis of the prepolymerization of palm-based polyurethane. *Solid State Sci Technol* 2010;18(2):1-8.

5. Hatchett DW, Kodippili G, Kinyanjui JM, Benincasa F, Sapochak L. FTIR analysis of thermally processed PU foam. *Polym Degrad Stab* 2005;87(3):555-61. [DOI: 10.1016/j.polymdegradstab.2004.10.012]

6. Tang Q, Gao K. Structure analysis of polyether-based thermoplastic polyurethane elastomers by FTIR, ^{1}H NMR and ^{13}C NMR. *Int J Polym Anal Charact* 2017;22(7):569-74. [DOI: 10.1080/1023666X.2017.1312754]